

EFFECTS OF SURFACE FINISH ON FATIGUE IN AUSTENITIC STAINLESS STEELS

Masatoshi Kuroda*, T. James Marrow and Andrew H. Sherry
Materials Performance Centre, School of Materials
University of Manchester
Grosvenor Street, Manchester M1 7HS, UK
*Corresponding Author (Masatoshi.Kuroda@manchester.ac.uk)

ABSTRACT

This paper reports an on-going research programme to understand the effects of the surface finish on fatigue in Type 304 austenitic stainless steels. This programme aims to establish a mechanistic model for the surface and microstructure effects on fatigue. A mechanistic model originally proposed by Navarro and Rios (N-R model) was selected as the most suitable generic model to study the effect of the surface finish on fatigue. The response surface methodology was used to prepare fatigue specimens with designed surface characteristics. The predictions of the machined specimens overestimated the observed fatigue limit significantly. A modification of the model to take better account of the near-surface microstructure and properties is required for accurate predictions of fatigue crack initiation in austenitic stainless steels.

Introduction

Austenitic stainless steels are important materials in light water reactors (LWRs), with a requirement for strength and corrosion resistance [1]. The fatigue behaviour has been reported to be influenced by surface roughness, strain hardening, microstructure and residual stress, which are all influenced by working of the surface [2, 3]. However, the available data in the literature is complicated by the interactions of these factors, which results in difficulty in deriving a fundamental understanding of the mechanism. This paper describes an on-going research programme to fully understand the effects of the surface finish on fatigue in Type 304 austenitic stainless steels. This programme aims to establish a mechanistic model for the surface/microstructure effects on fatigue.

This research programme can be classified into the following six topics. These are introduced in this paper, with further details published elsewhere [4-6].

- Identification of a suitable fatigue model for this programme [4]
- Design and preparation of fatigue specimens with controlled surface characteristics [5]
- Characterisation of surface/material properties of the fatigue specimens [4,6]
- Implementation of the fatigue model using the observed surface/material properties to predict fatigue behaviour [4]
- Comparison of the fatigue limit, observed by staircase method, with the model prediction [6]
- Post-mortem examination of the fatigue specimens and comparison with the model prediction [4,6]

Identification of a Fatigue Model

In order to identify the most suitable model for this programme among the existing short fatigue crack models, a literature review was carried out [4]. The generic mechanistic model for the behaviour of a short crack nucleus, originally proposed by Navarro and Rios [7-15] and which has been referred to as the N-R model, was selected. This model is basically derived by modifying the Dugdale-BCS models [16, 17], and defines the threshold condition for the resultant crack tip stress to exceed the strength of the barrier to crack propagation at a grain boundary. In recent years, the original N-R model has been developed further and applied to engineering issues [18-31], such as shot peening effects on fatigue of aluminium alloys. The model includes the effects of residual stress and surface roughness, and the fatigue threshold stress (σ_{Li}) can be described by Equation (1) [18, 19]:

$$\sigma_{Li} = Z_i \left(\sigma_1^i + \frac{m^i}{m^1} \frac{\sigma_{FL}}{\sqrt{i}} \right) \quad (1)$$

where i is the number of half grains covered by the crack; σ_1^i is the closure stress; Z_i is the notch influence factor; m^i/m^1 is the grain orientation factor which varies from 1 to 3.07 (Taylor Value [32]) for face centred cubic polycrystalline metals; σ_{FL} is the intrinsic fatigue limit for smooth specimens without any residual stress. The closure stress can be obtained by integrating the depth profile of the residual stress $f(RS)$ using Equation (2) [18, 19]:

$$\sigma_1^i = \frac{1}{i} \int_0^i f(RS) di \quad (2)$$

The notch influence factor is given in Equations (3) and (4) [20-22]:

$$Z_i = \frac{\sqrt{iD/2}}{\alpha + \beta} \left[\frac{\beta}{\lambda_i} + \frac{\alpha}{\sqrt{1 + \lambda_i^2}} \right]^{1/2} \quad (3)$$

$$\lambda_i = \frac{1}{\alpha^2 - \beta^2} \left[\alpha \sqrt{(\alpha + iD/2)^2 - \alpha^2 + \beta^2} - \beta(\alpha + iD/2) \right] \quad (4)$$

where α is the depth of the notch; β is the half-width of the notch; D is the grain size. In the present study, the profiles of the roughness on the specimen surfaces were interpreted as a series of micro-notches.

Several empirical relationships describing the grain orientation factor, m^i/m^1 , have been reported for mild steels and aluminium alloys [12, 15, 23], but not for stainless steels. In this study, in the absence of a more suitable relationship, the grain orientation factor was approximated by the following formulae [21, 22]:

$$\frac{m^i}{m^1} = \frac{\sqrt{\bar{a}_0}}{\left(i^f + \bar{a}_0^{-f} - 1\right)^{\frac{1}{2f}}} \sqrt{i} \quad (5)$$

$$\bar{a}_0 = \frac{a_0}{D/2} \quad (6)$$

$$a_0 = \frac{1}{\pi} \left(\frac{K_{th\infty}}{Y \cdot \sigma_{FL}} \right)^2 \quad (7)$$

where f is a fitting parameter, the value of which is reported to be 2.5 for steels [21, 22]; Y is a dimensionless constant that depends on geometry and mode of loading where $Y=1$ is set from the outset; $K_{th\infty}$ is the threshold stress intensity factor for long cracks is estimated using the following empirical relationship by Murakami et al. [33]:

$$K_{th\infty} = 1.65 \times 10^{-3} (H_V + 120) \left(\sqrt{\text{area}} \right)^{\frac{1}{3}} \quad (8)$$

where $K_{th\infty}$ is in $\text{MPa}\sqrt{\text{m}}$; $\sqrt{\text{area}}$ is in microns, and assumed to be 1000 μm in this study in accordance with Ref. [24]; H_V is the Vickers hardness of the material, here measured as the micro-hardness.

Design and Preparation of Fatigue Specimens

In order to study the effect of the surface finish on the fatigue behaviour quantitatively, fatigue specimens with controlled values of the roughness, hardness and residual stress should be prepared. An investigation was undertaken to develop a technique to prepare fatigue samples of austenitic stainless steels with designed surface characteristics. The response surface methodology (RSM) coupled with central composite design (CCD) [34, 35] was employed to design fatigue specimens with controlled surface characteristics. Simple cylindrical specimens having various surface characteristics were first produced by changing the final cutting conditions (spindle speed, feed rate and cutting depth) of the lathe. Since tool wear is significant in austenitic stainless steels due to their high work hardening capacity and low thermal conductivity [36, 37], wear effects were minimised by replacing the tool tip for every specimen prior to the final cut. The surface characteristics of the roughness, hardness and residual stress on the specimens were measured, and statistical analysis (ANOVA) was employed to obtain a response surface model.

The response surface model employed in the analysis could adequately represent the largest peak to valley height (roughness R_y) and the axial surface residual stress, but a good fit was not always achieved for the mean spacing of adjacent local peaks (roughness S) and the micro-hardness. The best fits for the roughness R_y and the axial surface residual stress σ_y , obtained by the ANOVA are given in Equations (9) and (10), respectively:

$$R_y = -1.03 - 1.90 \times 10^{-3} A + 57.2B + 5.45C - 2.48 \times 10^{-6} A^2 + 149B^2 - 0.239C^2 + 0.0235AB + 4.06 \times 10^{-3} AC - 11.3BC \quad (9)$$

$$\sigma_y = -715 + 0.365A + 5370B - 218C - 6.65 \times 10^{-5} A^2 - 9960B^2 + 27.4C^2 - 0.0618AB - 0.0594AC + 177BC \quad (10)$$

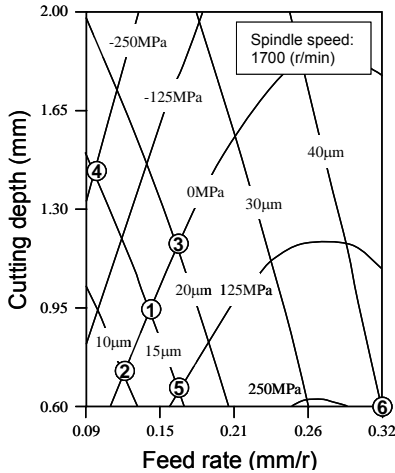


Figure 1. Response surface diagram obtained for lathe turning of cylindrical type 304 austenitic stainless steel specimens

Table 1. Cutting conditions for fatigue specimens.

Sample Type	Specimen 1	Specimen 2	Feed rate	Cutting depth	Spindle speed
	Code	Code	(mm/r)	(mm)	(r/mm)
0	0-1	0-2	0.10	0.4	1700
1	1-1	1-2	0.14	0.9	
2	2-1	2-2	0.12	0.7	
3	3-1	3-2	0.16	1.2	
4	4-1	4-2	0.10	1.4	
5	5-1	5-2	0.16	0.7	
6	6-1	6-2	0.32	0.6	

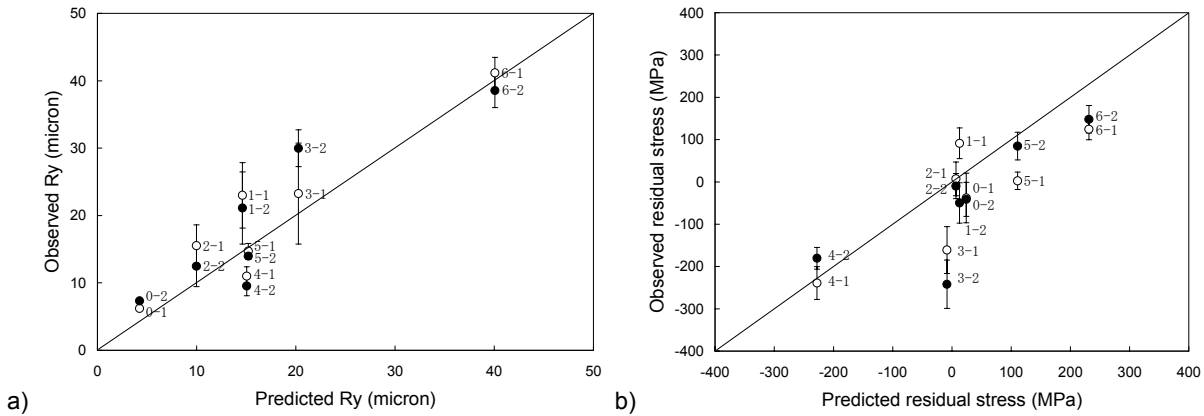


Figure 2. Comparison between the predicted and the measured value for a) surface roughness and b) axial surface residual stress

where A , B and C are the variables of the spindle speed (r/min), the feed rate (mm/r) and the cutting depth (mm), respectively. Figure 1 visualises Equations (9) and (10) and shows the interdependence of the roughness R_y and the axial surface residual stress. Based on the statistical analysis, specimens were identified on the response surface diagram, for example, as ① to ⑥, the cutting conditions of which are summarised in Table 1. Two fatigue specimens were therefore prepared for each specimen type, the codes of which are detailed in Table 1, to confirm whether the response surface model obtained on the cylindrical samples were valid for fatigue specimens. The observed values of the roughness R_y and the axial surface residual stress are given in Figure 2, compared with the values predicted by Equations (9) and (10), respectively. The prediction is in good agreement with the observed values for most conditions. The response surface methodology is demonstrated to be a novel approach to design fatigue specimens with controlled surface characteristics.

Characterisation of Surface/Material Properties

In order to implement the fatigue model, various surface/material properties of the fatigue specimens such as grain size, surface roughness, surface micro-hardness, residual stress depth profile and the fatigue limit for smooth specimens without

residual stress are required. In this section, the characterisation techniques and the data are summarised. The grain size was obtained by high-resolution electron backscatter diffraction (EBSD) in a Philips XL30 field emission gun-scanning electron microscope (FEG-SEM) equipped with an HKL Nordlys II detector and Channel 5 software. The grain sizes were calculated by the mean linear intercept method [38, 39] where the grain boundary was defined where adjacent pixels had a misorientation more than 15° . Coherent twin boundaries ($\Sigma 3$) were excluded from the analysis. Figure 3 shows the grain boundaries of as-received material where twin boundaries were identified as grey lines. The surface microstructure was not characterised.

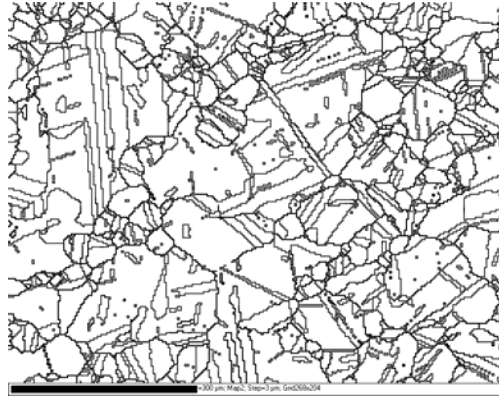


Figure 3. Observation of grain boundaries for as-received material characterised by EBSD where twin boundaries are identified by grey lines. The scale bar is 300 μm . The mean grain size is 40 μm .

A Hitachi S-3000N SEM coupled with Alicona-Mex stereographic imaging was used to visualise the 3D profiles of the surface roughness. Figure 4 shows typical surface profiles for the fatigue specimens. Statistically significant quantitative data was not obtained by this method, and the roughness R_a and S were also measured with a Taylor–Hobson Talysurf 50 surface profilometer, and verified against the stereographic profiles.

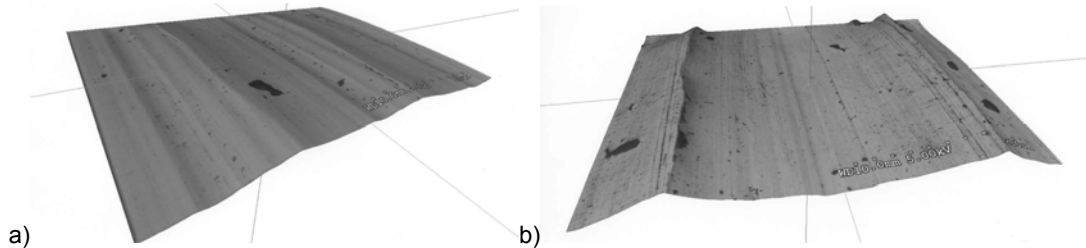


Figure 4. Qualitative 3D profiles of the surface roughness characterised by SEM coupled with stereographic imaging devices for the specimen codes of a) 0-2 and b) 6-2

The microhardness was measured by an Instron indentation instrument (Wilson Tukon 2100). The effect of the annealing and electropolishing for the sample Type 0 is compared in Figure 5. The figure reveals that strain hardened layer was removed by both electropolishing to remove 250 μm and annealing at 900°C for 10 minutes. The residual stress was measured with a Proto i-XRD X-ray diffractometer. Mn- $K\alpha$ radiation (20 kV, 4 mA) and the (311) diffraction plane (γFe) were used. The Young's modulus and Poisson's ratio employed were 193 GPa and 0.29, respectively. Depth profiles were obtained by successive removal of material with a Struers Lectropol-5 electropolishing unit at 20 V, in which the solution was 8% perchloric acid and 92% acetic acid. Figure 6 (a) shows the depth profiles of the axial residual stress for the machined samples, for which the specimen codes are listed in Table 1. No significant residual stresses were observed beyond a distance of approximately 250 μm from the surface. The axial residual stress profiles for the annealed Type 0 samples are given in Figure 6 (b) to illustrate the annealing effect. The lower annealing temperature of 425°C for 2 hours has no significant effect, but annealing at 900°C for 10 minutes effectively eliminates the machining induced residual stresses.

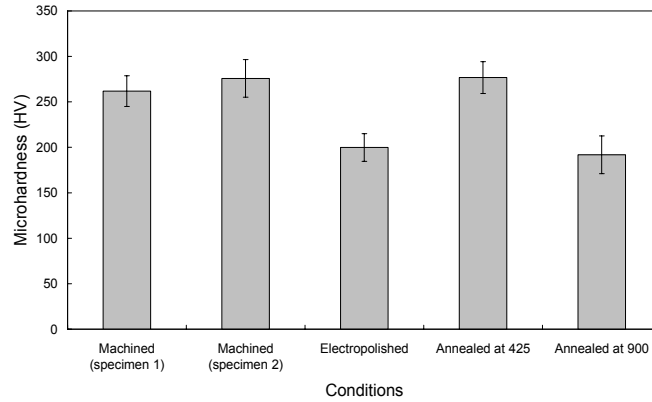


Figure 5. Comparison of the surface micro-hardness for the machined, electropolished and annealed Type 0 samples. The annealing times were 2 hours at 425°C and 10 minutes at 900°C.

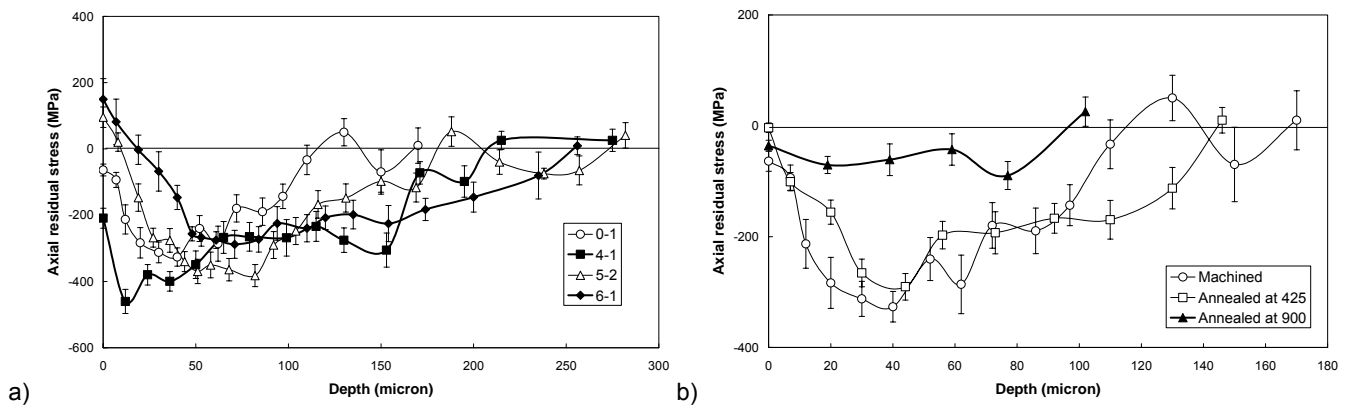


Figure 6. Depth profiles of axial residual stress for a) the machined samples and b) the annealed Type 0 samples. The annealing times were 2 hours at 425°C and 10 minutes at 900°C.

The fatigue limits were determined using a R.R. Moore rotating-bending machine by means of the staircase method [40] with 20 specimens, employing a step-width of 2 MPa. The fatigue endurance limit was set at 10^7 cycles. To obtain data for smooth specimens without residual stress effects, Type 0 fatigue specimens were first annealed at 900°C for 10 min to eliminate the residual stress due to the machining, and then electropolished to obtain a mirror finish (removal of approximately 150 μm). The fatigue limit of these annealed and electropolished samples was 298 MPa (± 2 MPa). Data was also obtained for the type 0 machined surface, and type 0 machined and annealed for 10 minutes at 900°C. The fatigue limits of the machined and annealed conditions were 295 MPa (± 2 MPa) and 295 MPa (± 4 MPa) respectively.

Implementation of the Fatigue Model

Figure 7 gives the predicted threshold stress profiles of the machined and annealed fatigue specimens, obtained by implementation of the fatigue model and the data obtained for grain size, surface roughness, micro-hardness, residual stress profile and the fatigue limit (298 MPa) for smooth specimens without residual stress. The maximum values of each profile, which are marked by open circles, correspond to the predicted fatigue limit. The crack length at stress amplitudes below the fatigue limit predicts a maximum arrested crack length that may be observed. The predicted fatigue limits are compared with the measured fatigue limits of the machined and the annealed specimens (Type 0) in the following section.

Comparison with the Fatigue Limit

The predicted fatigue limits shown in Figure 7 were 523 MPa and 270 MPa for the machined and annealed specimens, respectively. The surface roughness is therefore predicted to have a less significant effect than the residual stress profile. The prediction of the machined samples therefore overestimates the observed fatigue limit very significantly. A slight discrepancy, less than 10%, is also found for the predicted and observed fatigue limits of the annealed sample. Reasons for the disagreement between the model prediction and the experimental observations are discussed in the following section.

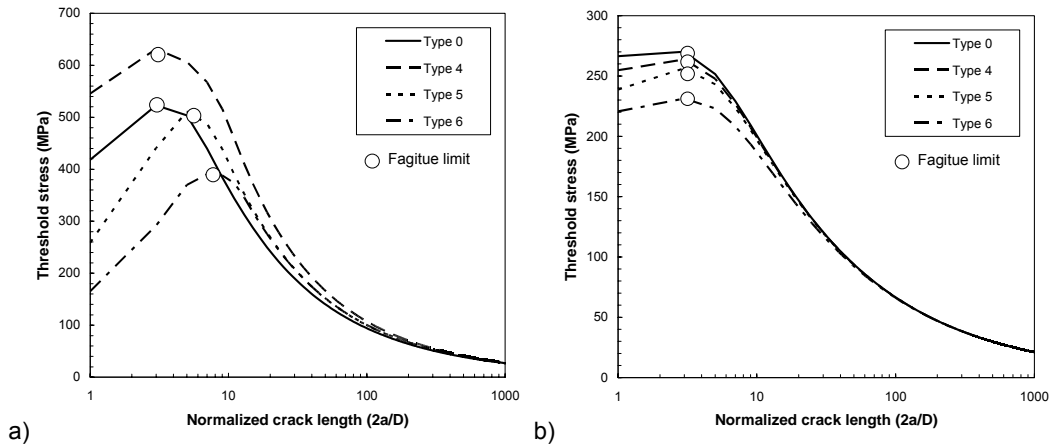


Figure 7. Threshold stress profiles predicted for a) the machined and b) the annealed (10 minutes at 900°C) specimens. The grain size, D , was 40 μm .

Post-Mortem Examination of the Fatigue Specimens

The fatigue model described in equation (1) assumes that the closure stress is superimposed in the threshold stress, which indicates that the proper estimation of the closure stress is important. Three possibilities can be considered for the disagreement of the fatigue limits between the model prediction and the experimental observations: (i) redistribution of the residual stress due to the fatigue loading, (ii) the reasonability of equation (2) to convert the residual stress into the closure stress and (iii) the validity of the microstructural parameters employed in the model.

Figure 8 compares the measured axial and circumferential surface residual stresses before and after fatigue. No significant change is observed, implying that high cycle fatigue does not cause measurable redistribution of residual stress. Equation (2) is derived from continuum mechanics, which therefore neglects the effect of the grains. It is implicit in the N-R model that cracks are arrested at the grain boundaries where the local plasticity would be produced. Such plasticity could influence the local closure stress. Recently, the N-R model combined with crystal plasticity finite element models has been reported to consider the effect of the plasticity at the crack tip [41] for the prediction of crack growth rate, but not for the fatigue limit. The present authors propose to investigate this type of approach for the modification of the closure stress estimation, as part of future work.

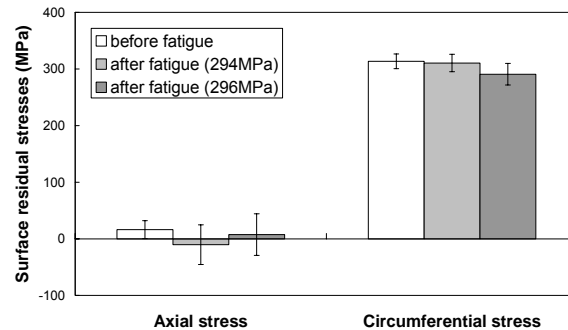


Figure 8. Comparison of the surface residual stresses measured before and after fatigue tests for Type 0 specimens

In order to consider whether the role of microstructure is adequately included in the model, the arrested crack behaviour has also been compared with the model predictions. Figure 9 shows cross-sections of the longest arrested cracks observed in post-fatigue (run-out) specimens for both the machined and annealed conditions. Similar cracks were observed in the electropolished specimens. The cracks are all significantly smaller than both the average grain size of the bulk of the microstructure (40 μm) and the expected arrest length (Figure 7). In the absence of a notch, the N-R model defines the fatigue limit as the stress amplitude below which a crack initiated within first surface grain is unable to propagate into the next grain. Crack initiation is thus assumed to be easier than propagation of the grain sized nucleus. The expected stable crack lengths in run-out specimens are therefore of the order of the grain size or more, which is inconsistent with the experimental observations. The observation of very short arrested cracks in all samples implies that in small specimens of austenitic stainless steels, crack initiation is difficult compared to crack propagation, and the fatigue limit, σ_{FL} , obtained for annealed, electropolished specimens is not the intrinsic resistance to propagation. This may explain the similarity between the measured fatigue limits of

all three surface conditions, in which the resistance to crack initiation may have been measured. Work is in progress to evaluate the near-surface deformation structures to further investigate this.

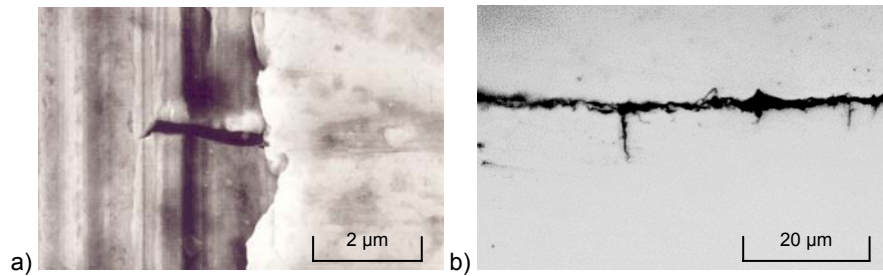


Figure 9. Arrested cracks in post-fatigue (run-out) specimens a) SEM observation of machined sample (propagation right to left), b) optical microscopy of annealed sample (propagation top to bottom).

Conclusions

A generic mechanistic fatigue model originally proposed by Navarro and Rios (N-R model) was selected as the most suitable model to study the effect of the surface finish on fatigue in austenitic stainless steels. The response surface methodology was demonstrated to be a novel approach to prepare fatigue specimens with designed surface characteristics. In order to predict the fatigue behaviour of the specimens prepared, the surface/material properties required to implement the model were characterised. The predictions for the machined specimens overestimated the observed fatigue limit significantly, indicating the importance of the machined surface on the initiation of fatigue cracks. Modifications to the model to take better account of near-surface microstructural parameters (including local plasticity and grain structure) are suggested as important factors in improving model predictions. Work is in progress to investigate a wider range of surface machined conditions.

Acknowledgments

This work has been financially supported by Serco Assurance of the United Kingdom. The views expressed are those of the authors, and not necessarily those of the research sponsors. The authors appreciate Ms. Judith Shackleton, Mr. Michael Faulkner, Mr. Trevor Jones, Mr. Neil Wardman, Mr. Adrian Handley, Mr. Stuart Morse, Mr. Ivan Easdon, Mr. Andrew Forrest and Dr. Andrew Peaker for their instructions on the experimental facilities. The authors would like to thank Mr. Christopher Hyde, Mr. Mark Harris, Mr. Gary Harrison and all the other Mechanical Workshop staffs for their care in specimen manufacture. Thanks are due to Dr. Paul Wood, Ms. Lai-Mei Li, Mr. Dirk Engelberg, Mr. Jonathan Duff, Dr. Kevin Tan, Dr. Andrew King, Dr. Anton Shterenlikht, Dr. Michael Trull and Dr. Joao Fonseca for their advice and help on the experiments and the modelling. The authors also appreciate the support of Professor Philip Withers.

References

1. Roberts, J. T. A., *Structural Materials in Nuclear Power Systems*, Plenum Press, New York (1984).
2. Yahata, N., Inukai, T. and Hayama, F., "Effect of surface working on the fatigue strength and wear of a hardened 13% Cr stainless steel", *Wear*, **80**, 89-100 (1982).
3. Yahata, N., "Effect of lapping on the fatigue strength of a hardened 13% Cr-0.34C stainless steel", *Wear*, **115**, 337-348 (1987).
4. Kuroda, M. and Marrow, T. J., "Prediction of the effects of surface finish on fatigue limit in austenitic stainless steels by short fatigue crack modeling", *Fatigue Fract. Engng Mater. Struct.*, to be submitted.
5. Kuroda, M. and Marrow, T. J., "Preparation of fatigue specimens with controlled surface characteristics", *J. Mater. Proc. Tech.*, submitted.
6. Kuroda, M. and Marrow, T. J., "Analyses of the effects of surface finish on fatigue limit in austenitic stainless steels by mechanistic modeling", 9th International Fatigue Congress, Atlanta, USA, to be presented.
7. Navarro, A. and De los Rios, E. R., "A model for short fatigue crack propagation with an interpretation of the short-long crack transition", *Fatigue Fract. Engng Mater. Struct.*, **10**, 169-186 (1987).
8. Navarro, A. and De los Rios, E. R., "A microstructurally-short fatigue crack growth equation", *Fatigue Fract. Engng Mater. Struct.*, **11**, 383-396 (1988).
9. Navarro, A. and De los Rios, E. R., "Short and long fatigue crack growth: a unified model", *Phil. Mag. A*, **57**, 15-36 (1988).
10. Navarro, A. and De los Rios, E. R., "An alternative model of the blocking of dislocations at grain boundaries", *Phil. Mag. A*, **57**, 37-42 (1988).
11. Navarro, A. and De los Rios, E. R., "Compact solution for a multizone BCS crack model with bounded or unbounded end condition", *Phil. Mag. A*, **57**, 43-50 (1988).
12. De los Rios, E. R. and Navarro, A., "Considerations of grain orientation and work hardening on short-fatigue-crack modeling", *Phil. Mag. A*, **61**, 435-449 (1990).

13. Xin, X. J., De los Rios, E. R. and Navarro, A., "Modeling strain hardening at short fatigue cracks", ESIS 13 (Edited by K J Miller and E R de los Rios), Mechanical Engineering Publications, London, 369-389 (1992).
14. Navarro, A. and De los Rios, E. R., "Fatigue crack growth modeling by successive blocking of dislocations", Proc. R. Soc. Lond. A, Math Phys. Sci., **437**, 375-390 (1992).
15. De los Rios, E. R., Xin, X. J. and Navarro, A., "Modeling microstructurally sensitive fatigue short crack growth", Proc. R. Soc. Lond. A, Math Phys. Sci., **447**, 111-134 (1994).
16. Dugdale, D. S., "Yielding of steel sheets containing slits", J. Mech. Phys. Solids, **8**, 100-104 (1960).
17. Bilby, B. A., Cottrell, A. H. and Swinden, K. H., "The spread of plastic yield from a notch", Proc. R. Soc. Lond. A, Math Phys. Sci., **272**, 304-314 (1963).
18. Curtis, S., De los Rios, E. R., Rodopoulos, C. A. and Levers, A., "Analysis of the effects of controlled shot peening on fatigue damage of high strength aluminium alloys", Int. J. Fatigue, **25**, 59-66 (2003).
19. Rodopoulos, C. A., Curtis, S. A., De los Rios, E. R. and SolisRomero, J., "Optimisation of the fatigue resistance of 2024-T351 aluminium alloys by controlled shot peening – methodology, results and analysis", Int. J. Fatigue, **26**, 849-856 (2004).
20. Navarro, A., Vallellano, C., De los Rios, E. R. and Xin, X. J., "Notch sensitivity and size effects described by a short crack propagation model", Engineering Against Fatigue, 63-72 (1999).
21. Vallellano, C., Navarro, A. and Dominguez, J., "Fatigue crack growth threshold conditions at notches part I: theory", Fatigue Fract. Engng Mater. Struct., **23**, 113-121 (2000).
22. Vallellano, C., Navarro, A. and Dominguez, J., "Fatigue crack growth threshold conditions at notches part II: generalization and application to experimental results", Fatigue Fract. Engng Mater. Struct., **23**, 123-128 (2000).
23. Curtis, S. A., SolisRomero, J., De los Rios, E. R., Rodopoulos, C. A. and Levers, A., "Predicting the interfaces between fatigue crack growth regimes in 7150-T651 aluminium alloy using the fatigue damage map", Mater. Sci. Eng. A, **344**, 79-85 (2003).
24. Vallellano, C., Mariscal, M. R., Navarro, A. and Dominguez, J., "A micromechanical approach to fatigue in small notches", Fatigue Fract. Engng Mater. Struct., **28**, 1035-1045 (2005).
25. De los Rios, E. R., Trull, M. and Levers, A., "Modeling fatigue crack growth in shot-peened components of Al 2024-T351", Fatigue Fract. Engng Mater. Struct., **23**, 709-716 (2000).
26. Rodopoulos, C. A. and De los Rios, E. R., "Theoretical analysis on the behaviour of short fatigue cracks", Int. J. Fatigue, **24**, 719-724 (2002).
27. Wei, L. W., De los Rios, E. R. and James, M. N., "Experimental study and modeling of short fatigue crack growth in aluminium alloy Al7010-T7451 under random loading", Int. J. Fatigue, **24**, 963-975 (2002).
28. Rodopoulos, C. A., De los Rios, E. R., Levers, A. and Yates, J. R., "A fatigue damage map for 2024-T3 aluminium alloy", Fatigue Fract. Engng Mater. Struct., **26**, 569-575 (2003).
29. Curtis, S. A., De los Rios, E. R., Rodopoulos, C. A. and Levers, A., "Analysis of the effects of controlled shot peening on fatigue damage of high strength aluminium alloys", Int. J. Fatigue, **25**, 59-66 (2003).
30. Rodopoulos, C. A., Choi, J-H., De los Rios, E. R. and Yates, J. R., "Stress ratio and the fatigue damage map – part I: modeling", Int. J. Fatigue, **26**, 739-746 (2004).
31. Rodopoulos, C. A., Choi, J-H., De los Rios, E. R. and Yates, J. R., "Stress ratio and the fatigue damage map – part II: the 2024-T351 aluminum alloy", Int. J. Fatigue, **26**, 747-752 (2004).
32. Taylor, G. I., "Plastic strain in metals", J. Inst. Metals, **62**, 307-324 (1938).
33. Murakami, Y. and Endo, M., "Effects of hardness and crack geometries on ΔK_{th} of small cracks emanating from small defects", EGF Pub.1 (Edited by K J Miller and E R de los Rios), Mechanical Engineering Publications, London, 275-293 (1986).
34. Montgomery, D. C., Design and Analysis of Experiments, John Willey & Sons, New York (1997).
35. Myers, R. H. and Montgomery, D. C., Response Surface Methodology, John Willey & Sons, New York (1995).
36. Korkut, I., Kasap, M., Ciftci, I. and Seker, U., "Determination of optimum cutting parameters during machining of AISI 304 austenitic stainless steel", Mater. Des., **25**, 303-305 (2004).
37. Tekiner, Z. and Yesilyurt, S., "Investigation of the cutting parameters depending on process sound during turning of AISI 304 austenitic stainless steel", Mater. Des., **25**, 507-513 (2004).
38. Humphreys, F. J., "Grain and subgrain characterisation by electron backscatter diffraction", J. Mater. Sci., **36**, 3833-3854 (2001).
39. Humphreys, F. J., "Characterisation of fine-scale microstructures by electron backscatter diffraction (EBSD)", Scripta Materialia, **51**, 771-776 (2004).
40. Maennig, W., "Planning and evaluation of fatigue tests", In: ASM handbook Vol.19: Fatigue and Fracture, ASM International, Materials Park, Ohio, USA (1996).
41. Lillbacka, R., Johnson, E. and Ekh, M., "A model for short crack propagation in polycrystalline materials", Eng. Fract. Mech., **73**, 223-232 (2005).